0090-9556/04/3210-1132–1138$20.00
DRUG METABOLISM AND DISPOSITION
Vol. 32, No. 10
638/1175656
DMD 32:1132–1138, 2004
Printed in U.S.A.

PLASMA PHARMACOKINETICS AND METABOLISM OF THE HISTONE DEACETYLASE INHIBITOR TRICHOSTATIN A AFTER INTRAPERITONEAL ADMINISTRATION TO MICE

L. Sanderson, G. W. Taylor, E. O. Aboagye, J. P. Alao, J. R. Latigo, R. C. Coombes, and D. M. Vigushin

Department of Cancer Medicine (L.S., J.P.A., R.C.C., D.M.V.), Section of Proteomics (G.W.T.), and Molecular Therapy Group (E.O.A., J.R.L.), Imperial College London (Hammersmith Hospital Campus), London, United Kingdom

Received May 14, 2004; accepted July 12, 2004

ABSTRACT:

Trichostatin A is a potent and specific histone deacetylase inhibitor with promising antitumor activity in preclinical models. Plasma pharmacokinetics of trichostatin A were studied following single-dose intraperitoneal administration of 80 mg/kg (high dose) or 0.5 mg/kg (low dose) to female BALB/c mice. Plasma trichostatin A concentrations were quantified by high performance liquid chromatography (HPLC)-UV assay (high dose) or by HPLC-multiple reaction monitoring assay (low dose). Trichostatin A was rapidly absorbed from the peritoneum and detectable in plasma within 2 min. C_{max} of 40 μg/ml and 8 ng/ml occurred within 5 min, followed by rapid exponential decay in plasma trichostatin A concentration with $t_{1/2}$ of 6.3 min and 9.6 min (high and low doses, respectively). Phase I metabolites at the high dose were identified by simultaneous UV and positive ion electrospray mass spectrometry. Trichostatin A underwent extensive metabolism: primary metabolic pathways were *N*-demethylation, reduction of the hydroxamic acid to the corresponding trichostatin A amide, and oxidative deamination to trichostatic acid. *N*-Monomethyl trichostatin A amide was the major plasma metabolite. No didemethylated compounds were identified. Trichostatic acid underwent further biotransformation: reduction and β-oxidation of the carboxylic acid, with or without *N*-demethylation, resulted in formation of dihydro trichostatic acid and dinor dihydro trichostatic acids. HPLC fractions corresponding to trichostatin A and *N*-demethylated trichostatin A exhibited histone deacetylase-inhibitory activity; no other fractions were biologically active. We conclude that trichostatin A is rapidly and extensively metabolized in vivo following intraperitoneal administration to mice, and *N*-demethylation does not compromise histone deacetylase-inhibitory activity.

Trichostatin A and its glucopyranosyl derivative trichostatin C are hydroxamic acids that were first isolated from cultures of *Streptomyces hygroscopicus* as antifungal antibiotics active against *Trichophyton sp*. (Tsuji et al., 1976; Tsuji and Kobayashi, 1978). Trichostatin A was subsequently found to exhibit potent cytostatic and differentiating activity at nanomolar concentrations against Friend murine erythroleukemia cells in culture (Yoshida et al., 1987). Later work identified similar antiproliferative activity against a broad range of human tumor-derived cell lines (reviewed in Vigushin and Coombes, 2004). Stereoselective synthesis of the enantiomers of trichostatin A and subsequent analysis showed that the natural configuration is *R*-(+)-trichostatin A, and *S*-(−)-trichostatin A is 70 times less biologically active (Yoshida et al., 1990a). Nuclear histones from cells treated with trichostatin A were found to be highly acetylated, and on pulse-chase analysis, this was due to decreased deacetylation rather than increased acetylation (Yoshida et al., 1990b). This observation led to the subsequent identification of histone deacetylase as the specific molecular target of trichostatin A (Yoshida et al., 1990b).

Grant support for this work from the National Translational Cancer Research Network and The Mandeville Trust is gratefully acknowledged. The Section of Proteomics is a joint facility funded by Imperial College Division of Medicine and the Medical Research Council Clinical Sciences Centre.

Article, publication date, and citation information can be found at http://dmd.aspetjournals.org.

doi:10.1124/dmd.104.000638.

The equilibrium between the opposing activities of histone acetyltransferase and histone deacetylase enzymes determines global cellular acetylation status (Struhl, 1998; Kouzarides, 1999). Reversible post-translational acetylation of ϵ-amino groups of highly conserved lysine residues in nucleosome core histones is important in the modification of chromatin superstructure and accessibility of the transcriptional apparatus to promoters of target genes (Pazin and Kadonaga, 1997; Wade et al., 1997; Wolffe, 1997). Histone deacetylase inhibition is in general associated with transcriptional activation of certain genes, e.g., *CDKN1A* (the gene for p21), but also repression of others, e.g., *CCND1*, which encodes cyclin D1 (Krajewski, 1999; Cress and Seto, 2000; Magnaghi-Jaulin et al., 2000). In addition to histones, other cellular proteins are also modified by acetylation, including transcription factors, e.g., p53 and E2F; nuclear hormone receptors, e.g., estrogen receptor α; and α-tubulin (reviewed in Vigushin and Coombes, 2004). Acetylation, therefore, is involved in many diverse cellular processes.

Trichostatin A is a potent, specific, and reversible histone deacetylase inhibitor at low nanomolar concentrations (Yoshida et al., 1990b). The biological consequences of histone deacetylase inhibition include reversion of transformed cell morphology and inhibition of cell proliferation by induction of G_1/S and G_2/M phase cell cycle arrest, differentiation, and/or apoptosis (reviewed in Vigushin and Coombes, 2004). Trichostatin A has potent broad spectrum antitumor activity against virtually all transformed cell types in culture including cell

ABBREVIATIONS: HPLC, high performance liquid chromatography; MS/MS, tandem mass spectrometry; ESP, positive ion electrospray ionization; MRM, multiple reaction monitoring.

lines derived from epithelial and hematological malignancies (Li et al., 1996; Lin et al., 1998; Kosugi et al., 1999; Saunders et al., 1999; Marks et al., 2000). We previously observed that trichostatin A had potent antitumor activity without apparent toxicity in vivo in the *N*-methyl-*N*-nitrosourea carcinogen-induced rat mammary cancer model (Vigushin et al., 2001). Trichostatin A also exhibits antitumor efficacy in the murine Lewis lung carcinoma model (Kim et al., 2001). Furthermore, trichostatin A is therapeutically active at nontoxic doses in various murine models of nonmalignant human disease including cardiomyocyte hypertrophy (Kook et al., 2003), premature parturition (Condon et al., 2003), glomerulonephritis in systemic lupus erythematosus (Mishra et al., 2003), and hepatic fibrosis induced by carbon tetrachloride (Elaut et al., 2002).

The biotransformation of trichostatin A in vitro has previously been reported (Elaut et al., 2002). Trichostatin A was rapidly and completely metabolized by rat hepatocytes; the major phase I biotransformation pathways were identified as *N*-demethylation and reductive amination of the hydroxamic acid; hydrolysis of trichostatin A to trichostatic acid was a minor pathway. In contrast, trichostatin A was slowly and incompletely metabolized by *N*-demethylation in rat and human microsome preparations, suggesting that trichostatin A reduction was catalyzed by nonmicrosomal enzymes. An intact hydroxamic acid function suggested that the *N*-demethylated trichostatin A metabolites may be pharmacologically active. Here we report on the in vivo plasma pharmacokinetics of trichostatin A and characterization of its plasma metabolites after single-dose intraperitoneal administration to female BALB/c mice.

Materials and Methods

Chemicals and Reagents. Trichostatin A (7-[4-(dimethylamino)phenyl]-4,6-dimethyl-7-oxo-hepta-2,4-dienoic acid hydroxamide; ≥99% purity) was obtained from Wako Chemicals GmbH (Neuss, Germany). HPLC (far UV) grade acetonitrile and Aristar grade formic acid were purchased from VWR International (Dorset, UK). All other reagents were from Sigma-Aldrich Ltd. (Dorset, UK).

Animals and Procedures. Female BALB/c mice (15–25 g) and female Ludwig Wistar rats (100–200 g) from Harlan Ltd. (Oxfordshire, UK) were maintained in accordance with the Animals (Scientific Procedures) Act, 1986. Animals were kept in controlled conditions of light, temperature, and humidity, and fed a standard diet with water ad libitum. Individual animals were weighed and dosed by intraperitoneal injection of trichostatin A, 80 mg/kg (mice) or 0.5 mg/kg (mice or rats) in 60 μl of 10% (v/v) dimethyl sulfoxide in filtered peanut oil. Syringes were flushed with an aqueous solution of bovine heparin (5000 U/ml). Animals were anesthetized with isoflurane at 2, 3.5, 5, 10, 15, 20, 30, and 60 min, and 24 or 48 h postinjection, and blood was collected by cardiac

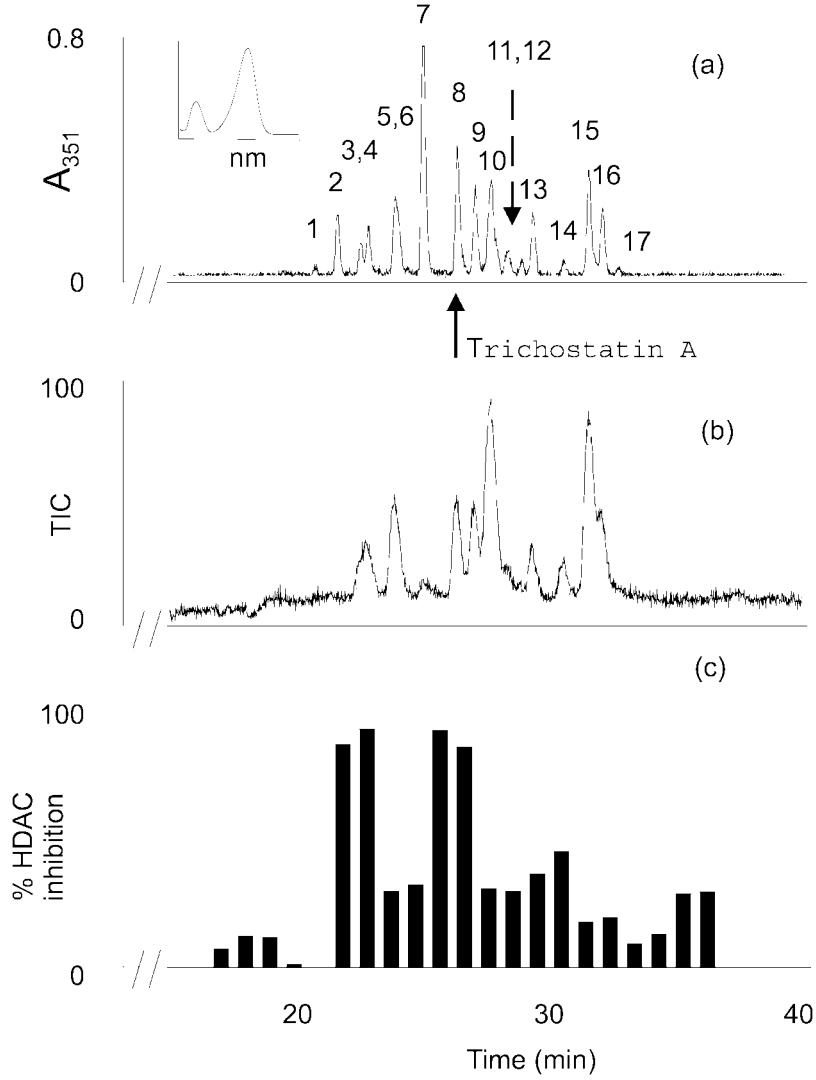

FIG. 1. HPLC profiles for the 20-min mouse plasma sample showing A_{351} UV absorbance (with the full UV spectrum of trichostatin A, inset) (a), electrospray mass spectrum total ion current (TIC) (b), and histone deacetylase (HDAC) activity (c). The elution position of trichostatin A is arrowed.

puncture into heparin-flushed syringes. Plasma was separated immediately by centrifugation (4750*g* for 5 min at room temperature), and samples were stored at −70°C until analyzed.

HPLC-UV Measurement of Trichostatin A in Plasma. HPLC analysis was carried out using a Jasco (Essex, UK) PS1585 HPLC system with an MD1510 diode array detector. Plasma aliquots (100 μl) were thawed and each was treated with 200 μl of acetonitrile. Samples were centrifuged at 4750*g* for 10 min at room temperature, and the supernatants were collected and then dried by rotary vacuum evaporation (without heating). Each sample was reconstituted in 150 μl of acetonitrile/water/formic acid, 10:90:0.1 (v/v); 100 μl was analyzed under HPLC system 1 conditions: samples were injected onto a HiChrom RPB, 5-μm, 100 × 2 mm column (Hichrom Ltd., Reading, UK) eluting at 0.3 ml/min with a linear gradient of acetonitrile/water/formic acid, 10:90:0.1 to 52:48:0.01 (v/v) over 40 min, followed by a 5-min gradient to 80:20:10 (v/v). Trichostatin A was quantified by measuring A_{351} and comparing against a five-point external standard curve.

HPLC-Multiple Reaction Monitoring (MRM) Assay. Trichostatin A was also measured by HPLC-MRM using a Jasco modular HPLC system coupled to a Micromass Quattro II triple quadrupole mass spectrometer (Waters, Altrincham, UK). 4-Dimethylamino-*N*-(6-hydroxycarbamoylhexyl)benzamide methyl ester was used as an internal standard. It was prepared from 4-dimethylamino-*N*-(6-hydroxycarbamoylhexyl)benzamide (M344; Merck Biosciences Ltd., Nottingham, UK) by methylation using trimethylsilyl diazomethane in ether for 1 h at room temperature. The standard was not purified before further use. Approximately 5 ng of internal standard was added to each plasma sample. After protein precipitation in acetonitrile and removal of excess solvents as above, samples were chromatographed under HPLC system 2 conditions on a HiChrom RPB column eluting at 250 μl/min with a 15-min linear gradient of acetonitrile/water/formic acid, 13.5:86.5:0.1 to 54:46:0.1 (v/v), followed by 3 min isocratically of acetonitrile/water/formic acid 54:46:0.1 (v/v). The eluate was passed into the positive ion electrospray ion source of the mass spectrometer with source temperature 75°C, cone potential 20 V, argon gas cell pressure 2×10^{-3} mbar, and collision energy 25 eV. Flow was monitored in the MRM mode monitoring transitions *m*/*z* 303 → 148 (trichostatin A) and *m*/*z* 336 → 148 (internal standard). A dwell time of 0.18 s and a mass span of 0.1 U were used for both transitions. A five-point extracted standard curve was prepared daily.

Identification of Metabolites. The remaining 20-min plasma samples from the high-dose study were combined and prepared for HPLC-diode array UV analysis. The HPLC eluant (split 1/13) was directed to a Quattro II triple quadrupole mass spectrometer for analysis by positive ion electrospray-MS mode. The ion source was operated at 75°C with a cone potential of 24 V. Scans (1 s/scan) were obtained between *m*/*z* 200 and 400. The remaining eluant was collected in 1-min fractions. Ten microliters of each fraction was injected directly onto the mass spectrometer for product ion analysis by positive ion electrospray-MS/MS. The collision gas was argon at a pressure of 2.1×10^{-3} mbar and the collision energy was set to 24 eV. The fractions were also analyzed on a Thermo LCQ Deca Ion Trap mass spectrometer (Thermo Electron, Franklin, MA) in the MS^n mode. The remaining fractions were dried under vacuum and each was resuspended in 50 μl of dimethyl sulfoxide for determination of histone deacetylase-inhibitory activity as previously described (Vigushin et al., 2001; Marson et al., 2004), with the modifications detailed below.

Histone Deacetylase Assay. The assay was performed in a final reaction volume of 200 μl. Two microliters of each fraction in dimethyl sulfoxide, 2 μl of dimethyl sulfoxide as a negative vehicle control, or 2 μl of trichostatin A at 100× the desired final concentration in dimethyl sulfoxide as positive control was added to 40 μl of 5× histone deacetylase buffer [50 mM Tris (pH 8.0), 750 mM NaCl, 50% (v/v) glycerol, 1 mM phenylmethylsulfonyl fluoride], 4 μl (40 μg total protein) of HeLa cell nuclear extract, and water to a total of 199 μl. After mixing by vortex and brief centrifugation (14,000*g* for 5 s at room temperature), the reaction mixture was incubated for 30 min at room temperature. The assay was then initiated by addition of 1 μl (37 kBq) of a ^{3}H-acetate-labeled synthetic peptide substrate corresponding to amino acids 14–21 of histone H4. After brief vortex and centrifugation as above, the reaction mixture was incubated for 60 min at room temperature. Fifty microliters of a quenching solution (1 M HCl/0.16 M acetic acid) was then added to stop the reaction. The released ^{3}H-acetate in each assay reaction was extracted into 600 μl of ethyl acetate. After mixing by vortex, the organic and aqueous phases were separated by centrifugation (14,000*g* for 1 min at room temperature). Duplicate 200-μl aliquots of the upper organic phase were transferred into separate scintillation vials each containing 5 ml of Hionic Fluor scintillant (Canberra Harwell Ltd., Didcot, UK) and the radioactivity in each was measured by β-scintillation counting. Each fraction was assayed in duplicate, and positive and negative control samples were assayed in triplicate. Histone deacetylase activity in each fraction was expressed as a percentage of the dimethyl sulfoxide negative control (taken as 100%)

Results

Trichostatin A chromatographed on HPLC (system 1) as a single A_{351} UV-absorbing peak with a retention time of 26.3 min and, under positive ion electrospray ionization, generated an intense $M + H^+$ ion at *m*/*z* 303. There were no other A_{351} UV-absorbing components in untreated mouse plasma. An HPLC-UV assay was developed for trichostatin A in plasma against a five-point external standard curve. Linearity was observed over the range 50 ng to 10 μg of trichostatin A ($r^2 > 0.999$), with the limit of detection set at 10 ng and the limit of quantification set at 50 ng. The assay was reproducible with intra-assay and interassay coefficients of variation of 12.5% ($n = 5$) and 18.5% ($n = 10$), respectively. Analytical precision was 89%.

HPLC-UV analysis of mouse plasma after intraperitoneal administration of trichostatin A showed the presence of a number of A_{351}-absorbing components; 17 UV-absorbing peaks were detected in the

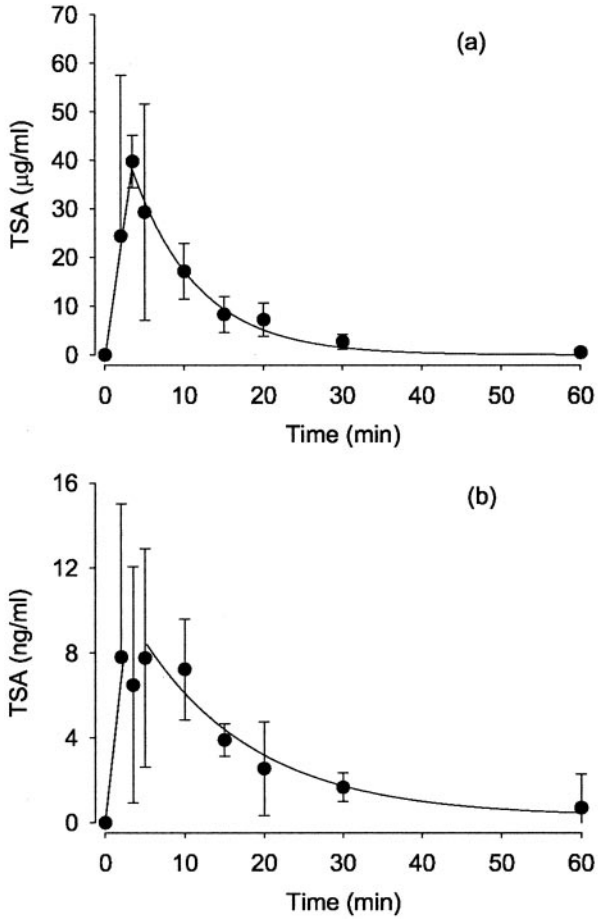

FIG. 2. Plasma pharmacokinetics of trichostatin A in mice following single-dose intraperitoneal administration. Mean and S.D. are shown. a, data from the HPLC-UV assay used for the higher dose (80 mg/kg) study. b, data from the HPLC-MRM assay used for the lower dose (0.5 mg/kg) study. Trichostatin A was completely eliminated by 24 h.

TABLE 1

HPLC-UV/ESP-MS-MS/MS analysis of trichostatin A and phase I metabolites

Peak	Retention Time	λ	M + H$^+$	MS/MS	Proposed Structure
1	20.75	344	N.D.[a]	N.D.	
2	21.69	341	254	N.D.	Not confirmed
3	22.56	341	289	289, 271, 259, 200, 164, **134**	*N*-Demethyl trichostatin A
4	22.93	346	248	248, 230, 202, 174, 108	Not confirmed
5	23.90	340	273	273, 256, 255, 245, 228, 212, 166, 149, **134**	*N*-Demethyl trichostatin A amide
6	23.97	344	250	250, 232, 108, MS^3 of 232 → 204, **134**	*N*-Demethyl dinor tetrahydro trichostatic acid
7	25.02	352	287	287, 270, 269, 177, 166, 149, **148**, 122, 121	Trichostatin A amide
8	26.40	350	303	303, 285, 270, 178, 148, 122	Trichostatin A
9	27.02	357	262	244, 216, 188, 122; MS^3 of 244 → 216, 188, **148**	Not confirmed
10a	27.60	~335–343	276	276, 258, 230, 151, **134**, 108	*N*-Demethyl dihydro trichostatic acid
10b	27.68		287	287, **148**	Trichostatin A amide isomer
10c	27.90		264	264, 246, 122, MS^3 of 246 → 218, **148**	Dinor tetrahydro trichostatic acid
11	28.32	341	274	**134**	*N*-Demethyl trichostatic acid
12	28.83	350	317	317, 299, 270,196, **148**, 122	Methyl trichostatin A
13	29.29	349	262	262, 244, **148**, 122	Dinor dihydro trichostatic acid
14	30.54	350	234	N.D.	Not confirmed
15	31.49	341	290	290, 272, 244, 187, 169, 141, **148**, 122	Dihydro trichostatic acid
16	32.01	349	288	288, 270, 244, 242, 178, 167, **148**, 122	Trichostatic acid
17	32.63	349	260	N.D.	Not confirmed

[a] N.D., mass spectrum not obtained.

20-min postinjection sample, (Fig. 1A). Trichostatin A (peak 8) was well separated from these components, and was identified and adjudged to be a single component by its characteristic UV spectrum (λ 250, 267, and 351 nm) and its ESP mass spectrum (M + H$^+$ at *m/z* 303). The other A_{351} components did not interfere with the measurement of trichostatin A using this HPLC-UV assay. To characterize the pharmacokinetics of trichostatin A in mice after intraperitoneal administration of 80 mg/kg (high dose), we measured the concentration of trichostatin A in plasma sampled at time points from 2 to 60 min; the results are shown in Fig. 2A. Trichostatin A was rapidly absorbed from the peritoneum and was detected in the plasma after only 2 min. After reaching a C_{max} of 40 μg/ml at 3.5 min, trichostatin A was also rapidly cleared, showing an exponential decay in plasma concentration with a half-life of 6.3 min. It was clear that, following this relatively high dose of trichostatin A (80 mg/kg), the concentration of trichostatin A in plasma at 60 min (>200 ng/ml) was well above the concentration necessary for histone deacetylase inhibition in vitro.

The HPLC-UV assay was insufficiently sensitive to monitor trichostatin A levels following low-dose administration, and so an HPLC-MRM assay was developed. An internal standard was prepared by methylating commercially available 4-dimethylamino-*N*-(6-hydroxycarbamoylhexyl)benzamide to form the monomethyl derivative. Using modified HPLC conditions (system 2), trichostatin A eluted at 13.3 min and the internal standard at 14.7 min. The internal standard generated an intense protonated molecular ion (M + H$^+$) at *m/z* 336 and fragmented by collision-induced dissociation to form the dimethylamino-phenylcarbonyl ion (*m/z* 148); this ion is also generated by collision-induced dissociation of the M + H$^+$ (*m/z* 303) ion of trichostatin A. These ion transitions (336→148 and 303→148) were then used as the basis for MRM assay. Using the HPLC-MRM assay, there was no evidence for trichostatin A in blank plasma. The assay had a limit of detection of 0.2 ng, limit of quantification of 0.4 ng, analytical precision of 96%, and intra-assay and interassay coefficients of variation of 10.6% and 12%, respectively. The assay was linear from 0.5 ng to 100 ng on column ($r^2 > 0.998$). In each case the internal standard was recovered in similar yield.

Using the assay, mouse plasma was analyzed at various times after administration of low-dose (0.5 mg/kg) trichostatin A. The data are shown in Fig. 2B; trichostatin A rapidly appears in plasma by 2 min (C_{max} 8 ng/ml) and decays exponentially between 5 and 60 min with a $t_{1/2}$ of 9.6 min. There was no evidence of trichostatin A in plasma samples taken at 24 h and 48 h. These pharmacokinetics are similar to those obtained with the high-dose study. Two rats were also treated with low-dose (0.5 mg/kg) trichostatin A. Although plasma trichostatin A was detected at 2 min, the maximum concentration reached was only 3.5 ng/ml. Trichostatin A had been completely eliminated by 24 h.

The 20-min plasma sample from the high-dose mouse study was selected for further examination of the other A_{351} components, and their UV spectra and ESP mass spectra were scrutinized (Fig. 1B; Table 1). The UV spectra were similar to that of trichostatin A, with characteristic absorbance values between 340 and 355 nm suggesting that they were metabolites containing the *N*-alkylated phenyl chromophore. Mass spectrometric examination defined the molecular weight of these metabolites, although it was clear that some UV peaks were associated with more than one component. Each of the metabolites was further examined by MS/MS. Under these conditions, the protonated molecular ion of trichostatin A at *m/z* 303 fragmented to generate a characteristic fragment ion at *m/z* 148 [$(CH_3)_2N{\cdot}C_6H_4{\cdot}CO^+$], which is diagnostic for the presence of *N*,*N*-dimethylaminophenylcarbonyl function. This ion was also present in a number of the metabolites (7, 8, 10b, 10c, 12, 13, 15, and 16). A second group of metabolites (3, 5, 6, 10a, and 11) generated a fragment at *m/z* 134 characteristic of an *N*-methylaminophenylcarbonyl group arising through *N*-demethylation. Metabolites 4 and 9 generated characteristic fragments at *m/z* 174 and 188. The molecular weight and fragmentation data (Table 1) allowed us to propose structures for the metabolites and indicated that metabolism of trichostatin A in vivo involves four metabolic pathways, which are illustrated in Fig. 3. These include the reduction of the hydroxamic acid group to give the corresponding amide, *N*-demethylation of the dimethylaminophenyl group, oxidative deamination of the hydroxamic acid group to give the corresponding acid, and reductive shortening of the carboxyl side chain. It would also appear that further derivatization of the hydroxamic acid group can occur. A species was observed (metabolite 12) exhibiting an M + H$^+$ at *m/z* 317, which fragmented to generate ions at 299 (–H_2O), 292 (–CO), 270 (–NH_2OCH_3), 196 [–$(CH_3)_2N{\cdot}C_6H_4$], 148 [$(CH_3)_2N{\cdot}C_6H_4{\cdot}CO^+$], 122 [$(CH_3)_2N{=}C_6H_6^+$]. This is consistent with an *N*-*O*-methylated trichostatin A. There was no conclusive evidence for either didemethylation or ring oxidation to produce aminophenyl or phenolic metabolites. Some minor components were observed with molecular weights consistent with didemethylation, but insufficient material was available for confirmatory MS/MS analysis.

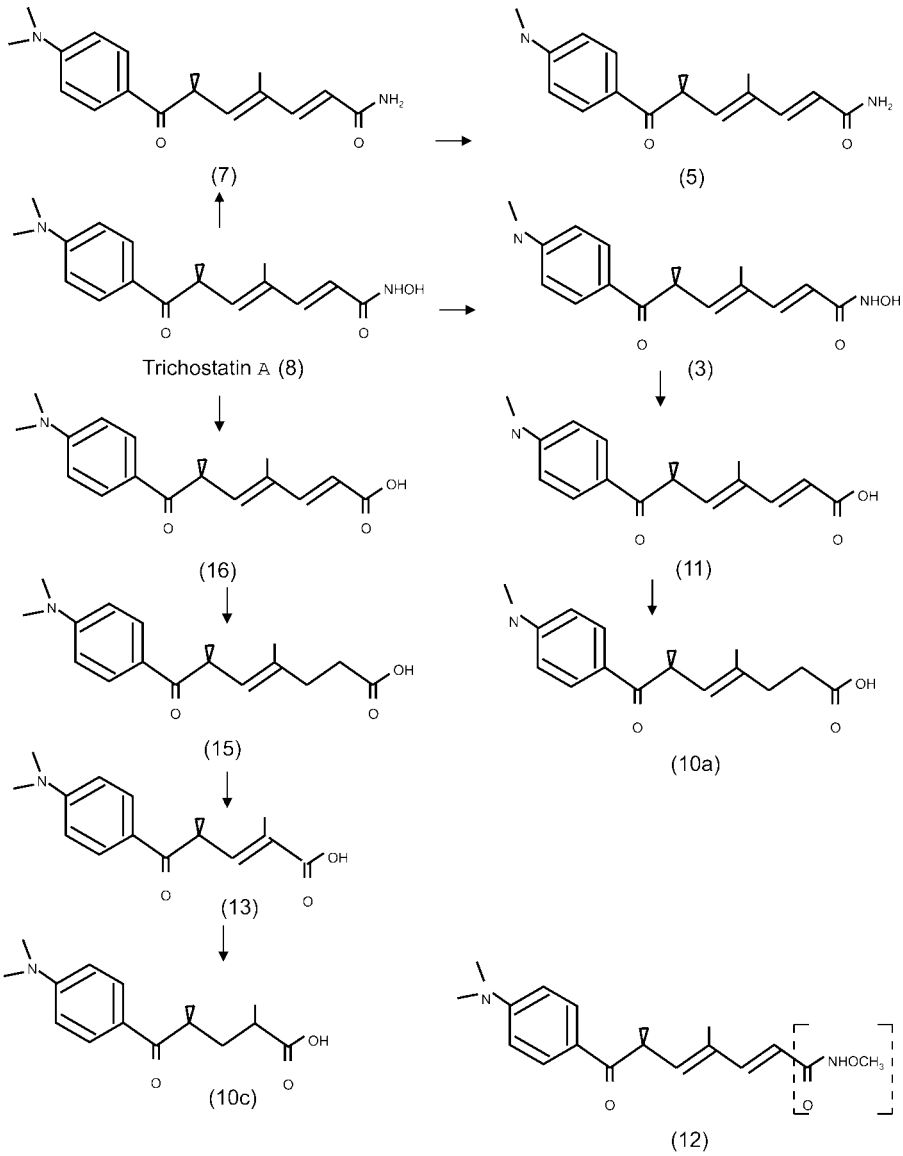

FIG. 3. Proposed phase I biotransformation pathways of trichostatin A and structures of the identified phase I metabolites formed in mouse plasma. Numbers in parentheses correspond to HPLC-UV peaks in Fig. 1A and Table 1.

Since the absorption coefficients of the identified metabolites were unknown and standards were not available, it was not possible to determine the absolute concentrations of the metabolites in plasma at the various time points. However, if it is assumed that the absorption coefficients do not differ significantly from that of trichostatin A, the peak areas can be used to estimate their concentration comparative to that of trichostatin A. The trichostatin A equivalent concentrations of metabolites that were completely resolved by the HPLC assay are shown in Fig. 4. *N*-Demethyl trichostatin A amide was the major metabolite produced, reaching a concentration of approximately 20 μg/ml (trichostatin A equivalents) after 60 min. It is unclear how long this compound persisted in the plasma because samples were not collected beyond this time point. Dihydro trichostatic acid and dinor dihydro trichostatic acid both reached a significant plasma concentration of approximately 13 μg/ml after 10 to 15 min; however, these compounds then declined rapidly.

The 20-min postinjection plasma sample was separated by HPLC into 1-min fractions. Each fraction was then tested for histone deacetylase-inhibitory activity in vitro (Fig. 1C). There were two main areas of activity, comprising fractions 20/21 and 24/25. Each of these fractions showed 92 to 99% inhibition of histone deacetylase enzyme activity, a level of activity comparable to that of 100 nM (approx. 30 ng/ml) trichostatin A (results not shown). HPLC-MS/MS analysis of these fractions showed that the earlier eluting activity was associated with *N*-demethyl trichostatin A, with trichostatin A accounting for the later eluting activity. Other metabolites were also present in these fractions.

Discussion

After intraperitoneal administration of trichostatin A in mice at two different doses, unchanged trichostatin A appeared in the circulation within 2 min, and was then rapidly cleared with first order kinetics for the high (80 mg/kg) and low (0.5 mg/kg) doses, respectively. Plasma pharmacokinetics were similar for both doses, suggesting that the metabolism and clearance are not materially affected by dosage. Plasma trichostatin A levels following high-dose administration remained above 200 ng/ml for up to 60 min, and this is well above the minimum required (0.5 ng/ml) to inhibit histone deacetylase activity

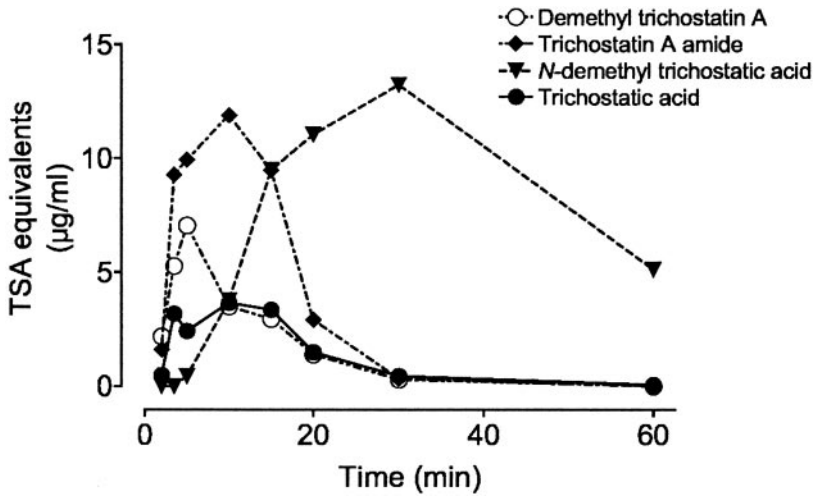

FIG. 4. Relative murine plasma concentrations (expressed as trichostatin A equivalents) of phase I metabolites of trichostatin A as a function of time. Mice received single intraperitoneal doses of 80 mg/kg trichostatin A. Trichostatin A equivalent concentrations of metabolites that were completely resolved by HPLC-UV assay were estimated from peak areas in plasma samples obtained at the indicated time points.

in vitro (Vigushin et al., 2001). In contrast, low-dose trichostatin A was only just present at bioactive concentrations at 60 min, and was completely eliminated by 24 h. The bioactive dose of trichostatin A in the *N*-methyl-*N*-nitrosourea-induced rat mammary cancer model is at least 40-fold lower than that in human breast cancer xenograft models in mice (D. M. Vigushin, unpublished observation). This is probably not due to pharmacokinetic reasons: after low-dose (0.5 mg/kg) intraperitoneal administration in two rats, trichostatin A appeared in plasma, but at only slightly lower levels than in the mouse (C_{max} 3.5 ng/ml), and was eliminated by 24 h.

Trichostatin A undergoes extensive metabolism in the mouse: the primary metabolic pathways are *N*-demethylation, reduction of the hydroxamic acid group to give the corresponding amide (trichostatin A amide), and oxidative deamination to trichostatic acid. The major metabolite in plasma is *N*-monomethyl trichostatin A amide. These results are in good agreement with a previous in vitro biotransformation study (Elaut et al., 2002) that showed both reduction and *N*-demethylation to be the major routes of biotransformation of trichostatin A in isolated rat and human hepatocyte suspensions, with *N*-demethylation occurring in the microsomal fraction. However, these authors found that further demethylation of the aminophenyl ring occurred, resulting in the formation of *N*-didemethylated trichostatin A amide as the major metabolite. In contrast, no didemethylated compounds were identified in the present study, although we observed some minor uncharacterized components with molecular weights consistent with didemethylation. It is not clear from our results how long *N*-monodemethyl trichostatin A amide persists in the plasma or whether it undergoes further demethylation after 60 min in vivo, since samples were not collected beyond this time point. Our results also showed that significant oxidative deamination of the hydroxylamine group occurred in vivo to form trichostatic acid. This was followed by reduction and β-oxidation of the carboxylic acid, with or without *N*-demethylation of the aminophenyl ring. This resulted in the formation of a number of metabolites with structures based on that of trichostatic acid, the most prevalent being dihydro trichostatic acid and dinor dihydro trichostatic acid. Whereas trichostatic acid was identified as a minor metabolite in both liver microsomes and hepatocytes isolated from either rats or humans (Elaut et al., 2002), these authors did not observe any further biotransformation of this compound. These results suggest that the reductive chain shortening of trichostatic acid-based compounds might occur via extrahepatic metabolic pathways.

Of the metabolites identified in the present study only *N*-demethyl trichostatin A had potent histone deacetylase-inhibitory activity in vitro. Other than trichostatin A, this was the only structure with an intact hydroxamic acid group, supporting the hypothesis that chelation of zinc at the base of the histone deacetylase enzyme active site by the hydroxamic acid group of trichostatin A prevents binding of the natural acetyl lysine substrate (Finnin et al., 1999).

Acknowledgments. We thank P. M. Loadman and J. A. Double for assistance.

References

Condon JC, Jeyasuria P, Faust JM, Wilson JW, and Mendelson CR (2003) A decline in the levels of progesterone receptor coactivators in the pregnant uterus at term may antagonize progesterone receptor function and contribute to the initiation of parturition. *Proc Natl Acad Sci USA* **100:**9518–9523.

Cress WD and Seto E (2000) Histone deacetylases, transcriptional control and cancer. *J Cell Physiol* **184:**1–16.

Elaut G, Torok G, Vinken M, Laus G, Papeleu P, Tourwe D, and Rogiers V (2002) Major phase I biotransformation pathways of trichostatin A in rat hepatocytes and in rat and human liver microsomes. *Drug Metab Dispos* **30:**1320–1328.

Finnin MS, Donigian JR, Cohen A, Richon VM, Rifkind RA, Marks PA, Breslow R, and Pavletich NP (1999) Structures of a histone deacetylase homologue bound to the TSA and SAHA inhibitors. *Nature (Lond)* **401:**188–193.

Kim MS, Kwon HJ, Lee YM, Baek JH, Jang JE, Lee SW, Moon EJ, Kim HS, Lee SK, Chung HY, et al. (2001) Histone deacetylases induce angiogenesis by negative regulation of tumor suppressor genes. *Nat Med* **7:**437–443.

Kook H, Lepore JJ, Gitler AD, Lu MM, Wing-Man Yung W, Mackay J, Zhou R, Ferrari V, Gruber P, and Epstein JA (2003) Cardiac hypertrophy and histone deacetylase-dependent transcriptional repression mediated by the atypical homeodomain protein Hop. *J Clin Investig* **112:**863–871.

Kosugi H, Towatari M, Hatano S, Kitamura K, Kiyoi H, Kinoshita T, Tanimoto M, Murate T, Kawashima K, Saito H, and Naoe T (1999) Histone deacetylase inhibitors are the potent inducer/enhancer of differentiation in acute myeloid leukemia: a new approach to anti-leukemia therapy. *Leukemia (Baltimore)* **13:**1316–1324.

Kouzarides T (1999) Histone acetylases and deacetylases in cell proliferation. *Curr Opin Genet Dev* **9:**40–48.

Krajewski WA (1999) Effect of in vivo histone hyperacetylation on the state of chromatin fibers. *J Biomol Struct Dyn* **16:**1097–1106.

Li W, Chen HY, and Davie JR (1996) Properties of chicken erythrocyte histone deacetylase associated with the nuclear matrix. *Biochem J* **314:**631–637.

Lin RJ, Nagy L, Inoue S, Shao W, Miller WH Jr, and Evans RM (1998) Role of the histone deacetylase complex in acute promyelocytic leukaemia. *Nature (Lond)* **391:**811–814.

Magnaghi-Jaulin L, Ait-Si-Ali S, and Harel-Bellan A (2000) Histone acetylation and the control of the cell cycle. *Prog Cell Cycle Res* **4:**41–47.

Marks PA, Richon VM, and Rifkind RA (2000) Histone deacetylase inhibitors: inducers of differentiation or apoptosis of transformed cells. *J Natl Cancer Inst* **92:**1210–1216.

Marson CM, Serradji N, Rioja AS, Gastaud SP, Alao JP, Coombes RC, and Vigushin DM (2004) Stereodefined and polyunsaturated inhibitors of histone deacetylase based on (2E,4E)-5-arylpenta-2,4-dienoic acid hydroxyamides. *Bioorg Med Chem Lett* **14:**2477–2481.

Mishra N, Reilly CM, Brown DR, Ruiz P, and Gilkeson GS (2003) Histone deacetylase inhibitors modulate renal disease in the MRL-lpr/lpr mouse. *J Clin Investig* **111:**539–552.

Pazin MJ and Kadonaga JT (1997) What's up and down with histone deacetylation and transcription? *Cell* **89:**325–328.

Saunders N, Dicker A, Popa C, Jones S, and Dahler A (1999) Histone deacetylase inhibitors as potential anti-skin cancer agents. *Cancer Res* **59:**399–404.

Struhl K (1998) Histone acetylation and transcriptional regulatory mechanisms. *Genes Dev* **12:**599–606.
Tsuji N and Kobayashi M (1978) Trichostatin C, a glucopyranosyl hydroxamate. *J Antibiot (Tokyo*) **31:**939–944.
Tsuji N, Kobayashi M, Nagashima K, Wakisaka Y, and Koizumi K (1976) A new antifungal antibiotic, trichostatin. *J Antibiot (Tokyo*) **29:**1–6.
Vigushin DM, Ali S, Pace PE, Mirsaidi N, Ito K, Adcock I, and Coombes RC (2001) Trichostatin A is a histone deacetylase inhibitor with potent antitumor activity against breast cancer in vivo. *Clin Cancer Res* **7:**971–976.
Vigushin DM and Coombes RC (2004) Targeted histone deacetylase inhibition for cancer therapy. *Curr Cancer Drug Targets* **4:**205–218.
Wade PA, Pruss D, and Wolffe AP (1997) Histone acetylation: chromatin in action. *Trends Biochem Sci* **22:**128–132.
Wolffe AP (1997) Transcriptional control. Sinful repression. *Nature (Lond)* **387:**16–17.
Yoshida M, Hoshikawa Y, Koseki K, Mori K, and Beppu T (1990a) Structural specificity for biological activity of trichostatin A, a specific inhibitor of mammalian cell cycle with potent differentiation-inducing activity in Friend leukemia cells. *J Antibiot (Tokyo*) **43:**1101–1106.
Yoshida M, Kijima M, Akita M, and Beppu T (1990b) Potent and specific inhibition of mammalian histone deacetylase both in vivo and in vitro by trichostatin A. *J Biol Chem* **265:**17174–17179.
Yoshida M, Nomura S, and Beppu T (1987) Effects of trichostatins on differentiation of murine erythroleukemia cells. *Cancer Res* **47:**3688–3691.

Address correspondence to: Dr. David Vigushin, Department of Cancer Medicine, 6th Floor MRC Cyclotron Building, Imperial College London (Hammersmith Hospital Campus), Du Cane Road, London W12 0NN, United Kingdom. E-mail: d.vigushin@imperial.ac.uk